# Text S1
# Regulating the many to benefit the few: role of weak small RNA targets

Daniel Jost, Andrzej Nowojewski, and Erel Levine
*Department of Physics, FAS Center for Systems Biology,*
*Harvard University, Cambridge, MA 02138, USA*

**Contents**

## Appendix A: Unified model for small RNA regulation

In this section, we present in details the model we used to study the srRNA-mediated regulation of principal targets in presence of auxiliary targets.

### 1. Stochastic model without auxiliary targets

The general picture of srRNA post-transcriptional regulation is well-described by modeling the dynamics of the number of srRNA $s$, of the number of principal mRNA targets $m$ and of the number of target proteins $p$, by a set of mass-action equations [1–5] where intrinsic fluctuations are captured by adding Langevin-like noises $\xi_i$ accounting for the stochasticity of the underlying reactions [6]:

$$\frac{ds}{dt} = \alpha_s - \beta_s s - ksm + \xi_s + \xi_k, \tag{A1}$$

$$\frac{dm}{dt} = \alpha_m - \beta_m m - ksm + \xi_m + \xi_k, \tag{A2}$$

$$\frac{dp}{dt} = \gamma m - \beta_p p + \xi_p, \tag{A3}$$

where $\alpha_i$ refers to the transcriptional rate of species $i$, $\beta_i$ to its degradation or turnover rate, and $\gamma$ to the translational rate of the target protein. $k$ represents the second-order kinetic constant between the srRNA and its target mRNA. Eq.A1 and A2 assume that the pairing between the srRNA and the mRNA leads to a rapid and full degradation of the complex. This type of active co-degradation is believed to occur for many prokaryotic small RNA-mRNA couples [7]. In eukaryotic pathways, evidence suggests that the degradation of the mRNA in the complex does not always yield the degradation of the srRNA [8]. However, in many cases the mRNA-srRNA pair is sequestered for considerable time, thus titrating the srRNA. Moreover, within the same framework it is easy to extend the model such that only a fraction of the srRNA is co-degraded with the mRNA (see section B 3). This does not affect the results of our work (see section C 3 c). In the following, for simplicity, we consider the minimal model given above, except in the sections B 3 and C 3 c.

Within the Langevin framework, each reaction is treated as an independent Poissonian process with white delta-correlated noise

$$\langle \xi_i(t) \rangle = 0, \tag{A4}$$

$$\langle \xi_i(t)\xi_j(t') \rangle = \delta_{ij} N_i \delta(t-t'), \tag{A5}$$

with $\delta_{ij}$ the Kronecker symbol, $\delta(t)$ the Dirac function, $N_s = \alpha_s + \beta_s\langle s\rangle$, $N_m = \alpha_m + \beta_m\langle m\rangle$, $N_k = k\langle s\rangle\langle m\rangle$ and $N_p = \gamma\langle m\rangle + \beta_p\langle p\rangle$, where $\langle\cdot\rangle$ represents the expectation value. The Langevin approach can be viewed as an approximation of the corresponding Master-equation for large numbers of molecules [9]. One of its advantage is that it allows to add extra contribution to the noise (such as diffusion or external noise) in a simple way (see below).

Within the same framework, transcriptional burstiness [10–13] can be efficiently accounted for by allowing the promoter $g$ to switch between two (on/off) states [6, 14]:

$$\frac{dg}{dt} = k_{\text{on}}(1-g) - k_{\text{off}} g + \xi_g, \tag{A6}$$

$$\text{with} \quad \langle \xi_g(t) \rangle = 0,$$

$$\langle \xi_g(t)\xi_g(t') \rangle = 2(k_{\text{on}} + k_{\text{off}})\langle g\rangle(1-\langle g\rangle)\delta(t-t')$$

$$\text{and} \quad \alpha_i = \alpha_i^0 g\,.$$

Here $k_{\text{on}}$ and $k_{\text{off}}$ are respectively the on and off rate of the promoter, and $\alpha_i^0$ the maximal transcription rate when the promoter is fully induced ($g = 1$). Arguably, the Langevin formalism is not natural to describe a two-state system. Indeed, instead of considering a binary switch dynamics between the two allowed states (on/off), $g$ is a continuous variable, and its equation of evolution (Eq.A6) is equivalent to a diffusion process in a quadratic potential centered around $\langle g\rangle$. However, steady-state values for the mean and the variance of the promoter occupancy are perfectly described by the Langevin framework (see Fig. S4). As seen below, this requirement is enough to provide excellent agreement with stochastic simulations in the regime where the linear noise approximation is adequate.

### 2. Effect of diffusion

This Langevin formalism implicitly assumes that the different species are well-mixed in the cell and that spatial correlations could be neglected. This is true so long as the typical diffusion time across the cell (of typical dimension $L$) $\tau_c = L^2/D$ is much shorter that the different relevant time-scales of the system. However, even in a well-mixed solution, diffusion plays an effective role by renormalizing the interaction constant between two reactants [15]

$$k = \frac{4\pi D\ell k^0/\Omega}{4\pi D\ell + k^0}, \tag{A7}$$

with $\Omega \propto L^3$ the volume of the cell, $D$ the relative diffusion constant between the two reactants, $\ell$ the typical scale of the reaction volume and $k^0$ the microscopic reaction rate which accounts for the local effective interaction between the two molecules. If $k^0 \gg D\ell$ then $k \approx 4\pi D\ell/\Omega$ and the macroscopic reaction is diffusion-limited. If $k^0 \ll D\ell$ then $k \approx k^0/\Omega$ and the interaction is reaction-limited.

Moreover, interaction between two molecules occurs in a very small volume ($\ell \ll L$). Therefore, diffusive arrival of molecules inside the reaction volume is also a stochastic process and leads to fluctuations in the local concentrations of the different species [14, 16, 17]. The corresponding variation in the rate $ksm$ would be given in the linear noise approximation [9] by

$$\delta(ksm) \approx k\left(\langle s\rangle \delta m + \langle m\rangle \delta s\right), \tag{A8}$$

with $\delta s$ ($\delta m$) the random variable characterizing the fluctuations of $s$ ($m$) due to diffusion. As long as the typical diffusion time in the reaction volume ($\sim l^2/D$) is much shorter than the other characteristic times of the system, terms in Eq.A8 could be considered as a white Langevin noise defined as

$$\langle \delta(ksm)\rangle = 0, \tag{A9}$$

$$\langle \delta(ksm)(t)\delta(ksm)(t')\rangle = k^2\tau(\langle s\rangle^2|\delta m|^2 + \langle m\rangle^2|\delta s|^2)\delta(t-t'), \tag{A10}$$

where $\tau$ is a typical time-scale, and $|\delta s|^2$ and $|\delta m|^2$ are the strengths of the diffusion fluctuations [16]

$$|\delta s|^2 = \frac{\Omega/(D\ell)}{\tau}\langle s\rangle \quad , \quad |\delta m|^2 = \frac{\Omega/(D\ell)}{\tau}\langle m\rangle \quad , \tag{A11}$$

and $D = D_s + D_m$ is the relative diffusion constant between the two species.

Grouping together all the terms related to the intrinsic fluctuations of the interaction between the srRNA and the mRNA, the diffusion noise can be captured by correcting the amplitude of the Langevin noise $\xi_k$ by

$$N_k = k\langle s\rangle\langle m\rangle\left(1 + \Sigma(\langle s\rangle + \langle m\rangle)\right), \tag{A12}$$

with $\Sigma = k\Omega/D\ell$. For diffusion-limited interactions, the prefactor $\Sigma$ is constant and independent of $D$. For reaction-limited interactions, $\Sigma \sim k^0/(D\ell) \ll 1$, and the diffusion noise is negligible.

### 3. Accounting for interactions with auxiliary targets

Next, we generalize the framework discussed above by considering the interaction between the srRNA and the auxiliary targets. These targets represent mRNAs molecules which could interact with the srRNA (i.e., containing a binding site) but whose mean levels are just weakly affected by the srRNA. Interaction between a srRNA and an auxiliary target leads to the formation of transient complexes. The kinetics of the numbers of auxiliary targets $n$ and of complexes $c$ follow the Langevin-like equations

$$\frac{dn}{dt} = \alpha_n - \beta_n n - k_a s n + k_d c + \xi_n + \xi_a + \xi_d, \tag{A13}$$

$$\frac{dc}{dt} = -\beta_c c + k_a s n - k_d c + \xi_c - \xi_a - \xi_d, \tag{A14}$$

where $\alpha_n$ is the total production rate over all auxiliary targets. $k_a = (4\pi D\ell k_a^0/\Omega)/(4\pi D\ell + k_a^0)$ is the association rate between the srRNA and the auxiliary targets and $k_d = (4\pi D\ell k_d^0)/(4\pi D\ell + k_a^0)$ the dissociation rate of the transient complex. The dissociation constant $K_d = k_d/k_a = k_d^0\Omega/k_a^0$ is independent of the diffusion constant. Degradation of

the complex is accounted for via $\beta_c$. The Langevin noises are characterized by their amplitudes: $N_n = \alpha_n + \beta_n\langle n\rangle$, $N_c = \beta_c\langle c\rangle$, $N_a = k_a\langle s\rangle\langle n\rangle(1 + (k_a\Omega/D\ell)[\langle s\rangle + \langle n\rangle])$ and $N_d = k_d\langle c\rangle$.

To account for the effect of the auxiliary targets on the srRNA level, one has to augment Eq.A1 by $(-k_a sn + k_d c + \beta_c(1-p_d)c + \xi_a + \xi_d + \xi_c')$, with $p_d$ the probability that the srRNA is also eliminated during the complex degradation, and $N_c' = \beta_c(1-p_d)\langle c\rangle$.

Note that for each type (principal and auxiliary) of targets, we focus on the dynamics of the whole ensemble. We do not consider possible heterogeneities (e.g. in the values of $k$ or $\alpha_m$) within each ensemble that, for example, may lead to hierarchical crosstalk between principal targets [1] (see Section C 4).

## Appendix B: Steady-state properties without auxiliary targets

In this section, we review the steady-state properties of srRNA regulation for a single target.

### 1. Mean levels

The mean steady-state levels could be estimated by setting to zero all the time derivatives and the Langevin noises present in our set of equations (Eq.A1-A3) [1]:

$$\langle s\rangle = \frac{\alpha_s - \alpha_m - \lambda + \sqrt{(\alpha_m - \alpha_s - \lambda)^2 + 4\alpha_m\lambda}}{2\beta_s}, \tag{B1}$$

$$\langle m\rangle = \frac{\alpha_m - \alpha_s - \lambda + \sqrt{(\alpha_m - \alpha_s - \lambda)^2 + 4\alpha_m\lambda}}{2\beta_m}, \tag{B2}$$

$$\langle p\rangle = \frac{\gamma\langle m\rangle}{\beta_p}, \tag{B3}$$

with $\lambda = \beta_s\beta_m/k$ the leakage rate which control the efficiency of the regulation [1]. These equations describe a linear-threshold response for the protein level (see Fig. S1 A) where three different regimes could be identified: (i) an unrepressed regime ($\alpha_s \ll \alpha_m$) where the srRNA-induced degradation of the mRNA target is small and the protein is expressed ($\langle p\rangle \approx p_{\max}$); (ii) a crossover regime around the threshold ($\alpha_s = \alpha_m$) where both the srRNA and the mRNA levels are low; and (iii) a repressed regime ($\alpha_s \gg \alpha_m$) where most of the mRNAs are targeted by the large srRNA pool and the expression of the protein is very low ($\langle p\rangle/p_{\max} \approx \lambda/\alpha_s \ll 1$) .

### 2. Fluctuations

The stochastic nature of the biochemical reactions composing gene regulation pathways leads to intrinsic fluctuations around the mean signal levels [18–20]. Total intrinsic fluctuations in the output protein level are the results of the propagation of the different sources of intrinsic noise along the regulatory pathway [20]. A canonical way to appreciate the strength of protein fluctuations is to consider the Fano factor $\nu = C_{p,p}/\langle p\rangle$, with $C_{p,p}$ the variance of $p$ at steady-state. $\nu$ is a measure of the noise-to-signal ratio, that allows estimating the deviation of the corresponding distribution of protein number from the Poisson limit ($\nu = 1$).

#### *a. Linear noise approximation (LNA)*

To compute $C_{p,p}$, we apply the linear noise approximation [9] to the set of Langevin equations. If we consider small perturbations around the steady-state ($s = \langle s\rangle + \delta s$, $m = \langle m\rangle + \delta m$ and $p = \langle p\rangle + \delta p$), the system of equations driving the evolution of the vector $\vec{\delta} = \{\delta s, \delta m, \delta p\}$ could be written in the general form

$$\frac{d}{dt}\vec{\delta} = J\vec{\delta} + \vec{\xi}, \tag{B4}$$

where $(J_{i,j})$ is the Jacobian of the full system and $\xi_i$ the different noise contributions ($\langle\xi_i\rangle = 0$, $\langle\xi_i(t)\xi_j(t')\rangle = N_{i,j}\delta(t-t')$).

There are two standard (and equivalent) approaches to estimate correlations between species in the weak noise limit. The first consists in taking the Fourier transform of Eq.B4, leading to

$$\tilde{\vec{\delta}} = A^{-1}\,\tilde{\vec{\xi}}, \tag{B5}$$

with $A_{i,i} = \imath\omega - J_{i,i}$, $A_{i,j} = -J_{i,j}$ $(i \neq j)$, and $\langle\tilde{\xi}_i(\omega)\tilde{\xi}_j^*(\omega')\rangle = 2\pi N_{i,j}\delta(\omega-\omega')$. The power spectrum $S(\omega)$ is then obtained from

$$\begin{aligned}\langle\tilde{\vec{\delta}}(\omega)\tilde{\vec{\delta}}^\dagger(\omega')\rangle &= A^{-1}\langle\tilde{\vec{\xi}}(\omega)\tilde{\vec{\xi}}^\dagger(\omega')\rangle(A^{-1})^\dagger \\ &= 2\pi\delta(\omega-\omega')[A^{-1}N(A^{-1})^\dagger] \equiv 2\pi\delta(\omega-\omega')S(\omega).\end{aligned} \tag{B6}$$

Using the Wiener-Khintchine theorem, the covariance matrix is then given by

$$C \equiv \langle\vec{\delta}\vec{\delta}^\dagger\rangle = \int\frac{d\omega}{2\pi}S(\omega) = \int\frac{d\omega}{2\pi}[A^{-1}N(A^{-1})^\dagger]. \tag{B7}$$

The second method starts by explicitly writing the time-derivative of the covariance matrix

$$\frac{d}{dt}C \equiv \frac{d}{dt}\langle\vec{\delta}\vec{\delta}^\dagger\rangle = JC + CJ^\dagger + \langle\vec{\delta}\vec{\xi}^\dagger + \vec{\xi}\vec{\delta}^\dagger\rangle. \tag{B8}$$

Formally, the solution of Eq.B4 is given by

$$\vec{\delta} = \exp[Jt]\vec{\delta}_0 + \int_{t_0}^{t} dt'\exp[J(t-t')]\vec{\xi}(t'). \tag{B9}$$

Therefore,

$$\begin{aligned}\langle\vec{\delta}\vec{\xi}^\dagger + \vec{\xi}\vec{\delta}^\dagger\rangle &= \exp[Jt]\langle\vec{\delta}_0\vec{\xi}^\dagger\rangle + \int_{t_0}^{t}dt'\exp[J(t-t')]\langle\vec{\xi}(t')\vec{\xi}^\dagger(t)\rangle + \langle\vec{\xi}\vec{\delta}_0^\dagger\rangle\exp[J^\dagger t] + \int_{t_0}^{t}dt'\langle\vec{\xi}(t)\vec{\xi}^\dagger(t')\rangle\exp[J^\dagger(t-t')] \\ &= \exp[Jt]\langle\vec{\delta}_0\rangle\langle\vec{\xi}^\dagger\rangle + \int_{t_0}^{t}dt'\exp[J(t-t')]\delta(t-t')N + \langle\vec{\xi}\rangle\langle\vec{\delta}_0^\dagger\rangle\exp[J^\dagger t] + \int_{t_0}^{t}dt'N\delta(t-t')\exp[J^\dagger(t-t')] \\ &= N.\end{aligned} \tag{B10}$$

Using this result in Eq.B8, one arrives at

$$\frac{d}{dt}C = JC + CJ^\dagger + N, \tag{B11}$$

(which can also be obtained using the $\Omega$-expansion of the Master-equation [9]). The steady-state covariance matrix is given by solving the linear system $JC + CJ^\dagger + N = 0$ (often referred to as the fluctuation-dissipation theorem).

In the following, analytical results were derived using the first method whereas numerical results were computed using the second.

### *b. Protein fluctuations*

The Fourier transform method applied to Eq.A3 gives

$$\langle|\delta\tilde{p}|^2\rangle = \frac{2\beta_p p}{\omega^2+\beta_p^2} + \frac{\gamma^2}{\omega^2+\beta_p^2}\langle|\delta\tilde{m}|^2\rangle, \tag{B12}$$

$$C_{pp} = \langle\delta p^2\rangle = \int\frac{d\omega}{2\pi}\langle|\delta\tilde{p}|^2\rangle = p + \gamma^2\int\frac{d\omega}{2\pi}\frac{\langle|\delta\tilde{m}|^2\rangle}{\omega^2+\beta_p^2}. \tag{B13}$$

The last equation illustrates that the noise in the protein level is the sum of a characteristic Poisson noise and of the propagation of the mRNA noise through a lowpass filter of frequency $\beta_p$. Generally speaking, one expects the protein lifetime to be longer than interaction time-scales and mRNA lifetimes. Therefore, the lowpass frequency can be considered much lower than other typical frequencies in the system, and Eq.B13 reduces to

$$C_{pp} = p + \frac{\gamma^2}{2\beta_p}\langle|\delta\tilde{m}|^2(0)\rangle. \tag{B14}$$

The Fourier transform method applied to the couple $(s, m)$ leads to

$$\delta\tilde{m} = \frac{(\imath\omega + \beta_s + km)\tilde{\xi}_m + (\imath\omega + \beta_s)\tilde{\xi}_k - km\tilde{\xi}_s}{(\imath\omega + \beta_s)(\imath\omega + \beta_m + ks) + km(\imath\omega + \beta_m)}. \tag{B15}$$

Accounting for transcriptional burstiness leads to the same expression if we renormalize $\tilde{\xi}_{s,m} \to \tilde{\xi}_{s,m} + \alpha^0_{s,m}\tilde{\xi}_{g_{s,m}}/(\imath\omega + k_{on_{s,m}} + k_{off_{s,m}})$.

Using Eq.B14 and B15 and after some algebra, we can find simple expressions for the Fano factor in the unrepressed and repressed regimes. In the unrepressed regime, the Fano factor is given by

$$\nu^{unrep} \approx (1 + b) + b\left(1 - \frac{\langle p\rangle}{p_{max}}\right)\left[\left(\frac{\alpha_m - \lambda}{\alpha_m + \lambda}\right) + \left(\frac{\alpha_m\beta_s\lambda}{(\alpha_m + \lambda)^2}\right)\left(\frac{\Omega}{2D\ell}\right)\right], \tag{B16}$$

where $b = \gamma/\beta_m$ is the protein burst size (average number of proteins produced per mRNA) and $p_{max} = \gamma\alpha_m/(\beta_p\beta_m)$ is the maximal mean protein number obtained when $\alpha_s = 0$. The first term of Eq.B16 reflects the burstiness of the translation of the mRNA [18]. Diffusion noise intervenes in the second (first-order) term and has only a very small effect on the global noise in this regime.

In the repressed regime, we find

$$\nu^{rep} \approx (1 + b^*) + b\beta_m\left(\frac{\Omega}{2D\ell}\right)\left(1 - \frac{b^*}{b}\right), \tag{B17}$$

where $b^* = b/(1 + k\langle s\rangle/\beta_m) = b\langle p\rangle/p_{max} \ll b$ is the effective protein burst size. $b^*$ is much smaller than the natural value $b$ since the effective lifetime of the mRNA ($[\beta_m + k\langle s\rangle]^{-1}$) is greatly reduced by srRNA-induced degradation. The last term in Eq.B17 is the signature of the diffusion noise (Eq.A12) which tends to increase the expression basal level. For slow diffusion (compared with $\beta_m$), the slow stochastic diffusion of a very low number of mRNA molecules can lead to relatively high fluctuations in the local mRNA concentration and diffusion noise may dominate. In the limit of high diffusion, intrinsic fluctuations are greatly suppressed by a strong srRNA regulation ($\nu^{rep} \ll \nu^{unrep}$).

In the crossover regime, the mRNA and srRNA levels are both very low. The ultra-sensitivity of the system leads to large (near critical) fluctuations [21] (see Fig. S1 B). Indeed, near the threshold, the cell state becomes broadly distributed and alternates between unrepressed and repressed states, yielding to a large distribution for the protein level with a high noise-to-signal ratio [22]. This effect is significantly enhanced by strong interaction ($k \gg 1$). In this regime, varying the diffusion modifies the strength of the fluctuations mainly by changing the sensitivity of the system via $k$ (Eq.A7).

#### *c. Comparison with stochastic simulations*

We now compare the results of the linear noise approximation to those of stochastic simulation. Simulations were implemented using the Gillespie algorithm [23]. Fig. S3A shows the good agreement between the solutions of the rate equations (Eqs.B1-B3) and of the full-stochastic system. Small deviations are observed around the threshold where correlations between the levels of srRNA and mRNAs are important. As already pointed out by Mehta et al [6], Fig. S3B shows the good quality of the LNA to describe the mean and the variance of the different species, even in the cross-over regime where numbers of molecules are low and the fluctuations are high. The position and amplitude of the peak of the Fano factor, predicted by the LNA, deviate only slightly from the result from Gillespie simulations. However, while the LNA well describes the behavior of the covariance matrix of the system, it is known [21] that the classic LNA fails to reproduce the bistable distribution due to the ultra-sensitivity of the system close to the threshold.

As discussed above, the LNA perfectly describes the steady-state values for the mean and the variance of the promoter occupancy even when we consider transcriptional burstiness (Fig. S4), despite the intrinsic binary nature of the promoter states.

### 3. Effect of recycling the srRNA

Here we assume that only a fraction $f$ of the srRNA is co-degraded with the principal target mRNA [24]. The system of mass-action equations describing the dynamics of $s$, $m$, $p$ and $c_0$ (number of srRNA-mRNA complexes) is

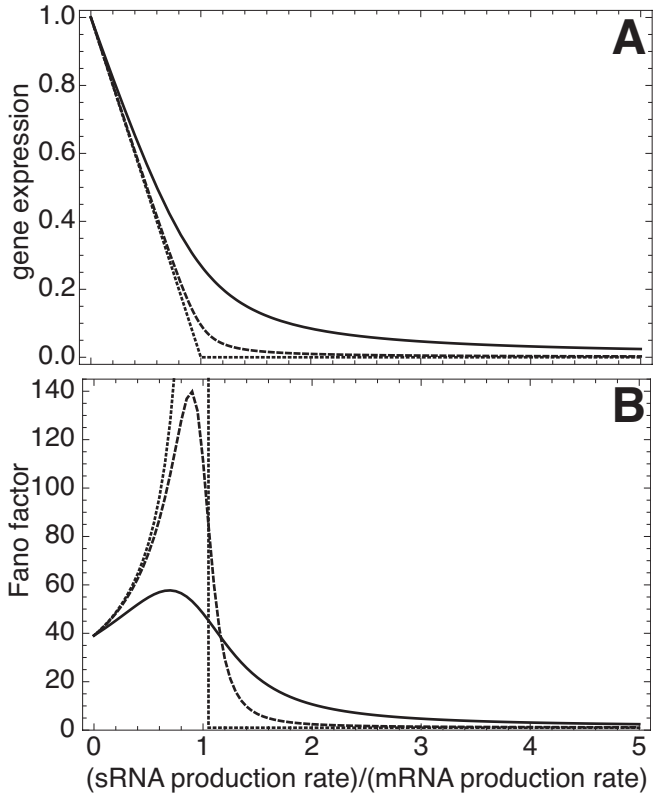


Fig. S1: Review of the steady-state properties of a protein regulated by a srRNA in the absence of auxiliary targets. Mean protein level (A) and the corresponding Fano factor (B) are plotted as a function of the ratio between the srRNA and the mRNA transcription rates for different values of the interaction rate k (full lines: 0.1 $min^{-1}$, dashed: 1, dotted: ∞). Strong interactions lead to sharp ("ultra-sensitive") linear-threshold response. Fixed parameters are (in $min^{-1}$) $\alpha_m = 1$, $\beta_m = 0.1$, $\beta_s = 0.1$, $\gamma = 4$, $\beta_p = 1/200$ (see SI Text, Sec.A for a detailed definition of each parameter).

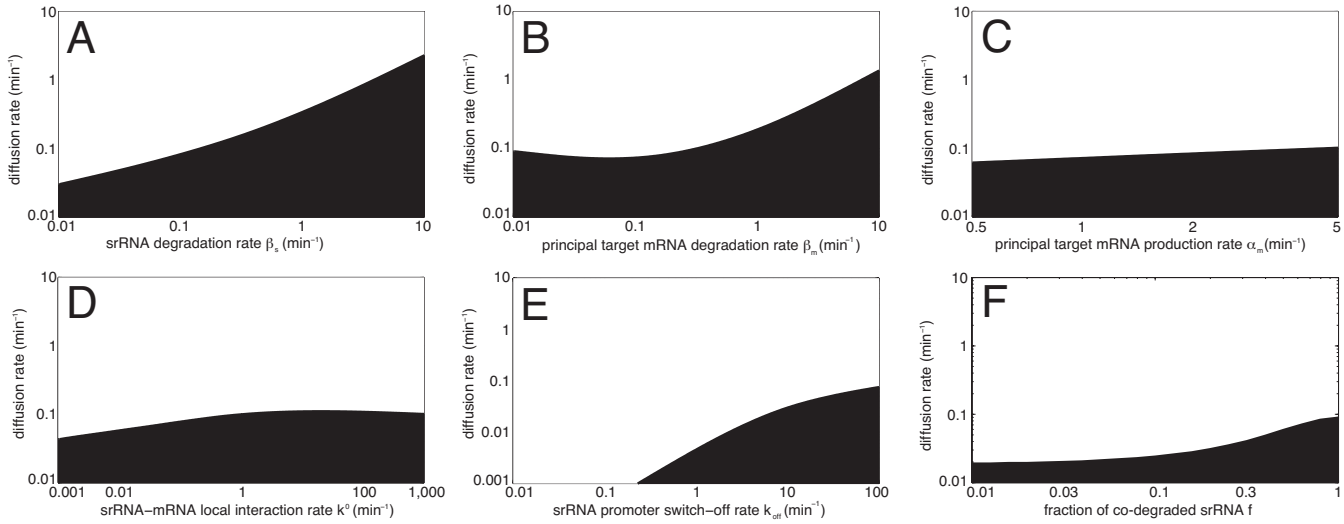


Fig. S2: Impact of parameters on the transition between fast and slow diffusion limit in presence of auxiliary targets. In the fast transport regions (white zones), auxiliary targets help maintaining a low level of intrinsic noise for the principal targets. In the slow transport regions (black zones), diffusion noise dominates and the presence of auxiliary targets increases the internal fluctuations of the principal targets. The frontier between fast and slow modes was computed using the notion of information capacity of the regulatory pathway (see SI Text Sec. C for details). In (E), we augment the burstiness of the srRNA promoter by decreasing the switch-off rate. Fixed parameters as in Fig. S1, completed by (in $min^{-1}$) $\beta_n = 0.1$, $\beta_c = 0$, $k_0 = 0.1$, $k_{a0} = 0.1$, $k_{d0} = 1$, (see SI Text Sec. A for a detailed definition of each parameter).

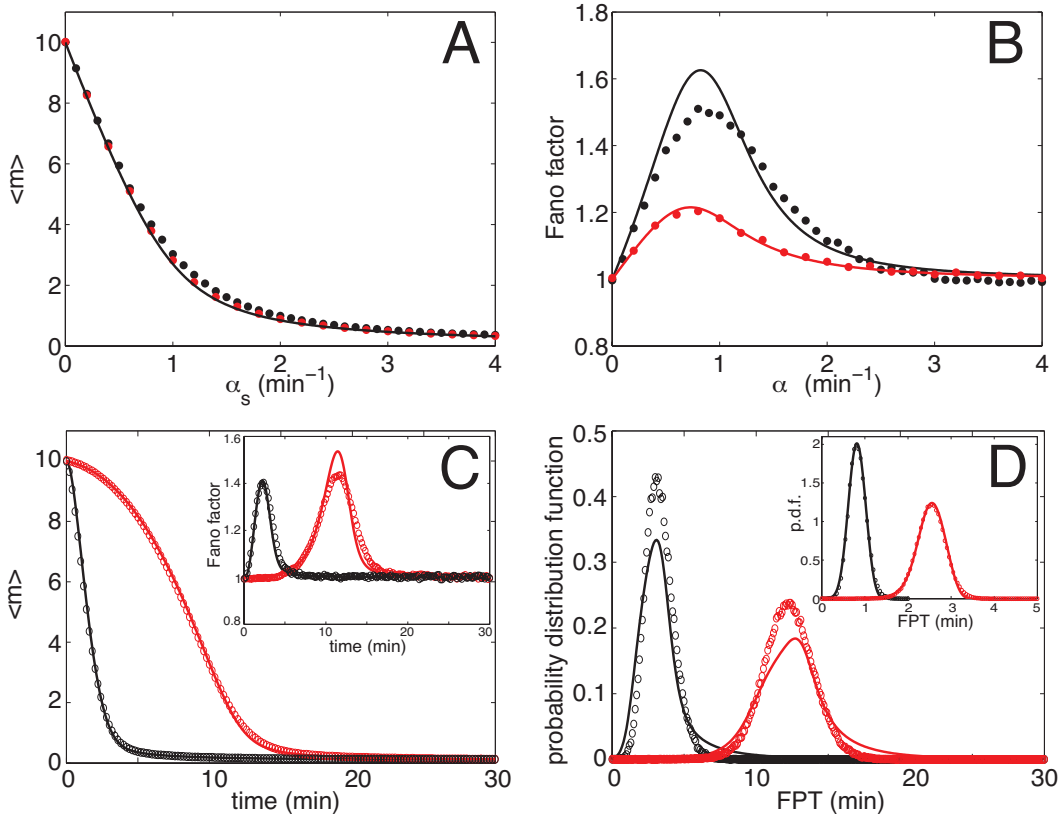


FIG. S3: Comparison of the linear-noise approximation (full lines) and stochastic simulations (dots/circles). Steady-state (A,B) and temporal response (C) for the mean number of principal targets $\langle m \rangle$ (A,C) and the corresponding Fano factor $\nu$ (B,inset in C) as a function of the srRNA production rate $\alpha_s$ (A,B) or time (C), in absence (black) or presence (red) of auxiliary targets ($\langle n \rangle = 10$ in A,B; and $n_{\rm tot} = 100$ in C,D). (D) Probability distribution function (p.d.f) of the first-passage time (FPT) for $m$ ($\alpha_m = 1$ min$^{-1}$) to reaches 0, after the activation of the srRNA transcription ($\alpha_s = 10$ min$^{-1}$) . The inset in D shows the p.d.f of the FPT for $m$ ($\alpha_m = 5$ min$^{-1}$) to reach $[\langle m \rangle(0)]/2$ ($\alpha_s = 50$ min$^{-1}$). Same parameters as in Fig. S1, completed by $k_a = k_d = 1$ min$^{-1}$ and $\beta_n = 0.1$ min$^{-1}$.

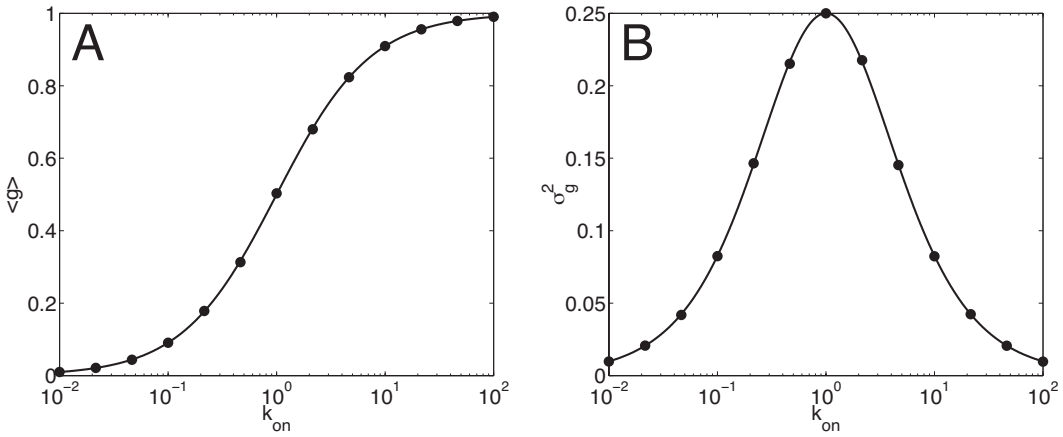


FIG. S4: Comparison of the linear-noise approximation (full lines) and stochastic simulations (dots) for the steady-state mean (A) and variance (B) of the promoter state $g$ (see Eq.A6) if one considers transcriptional burstiness in the model ($k_{\rm off} = 1$).

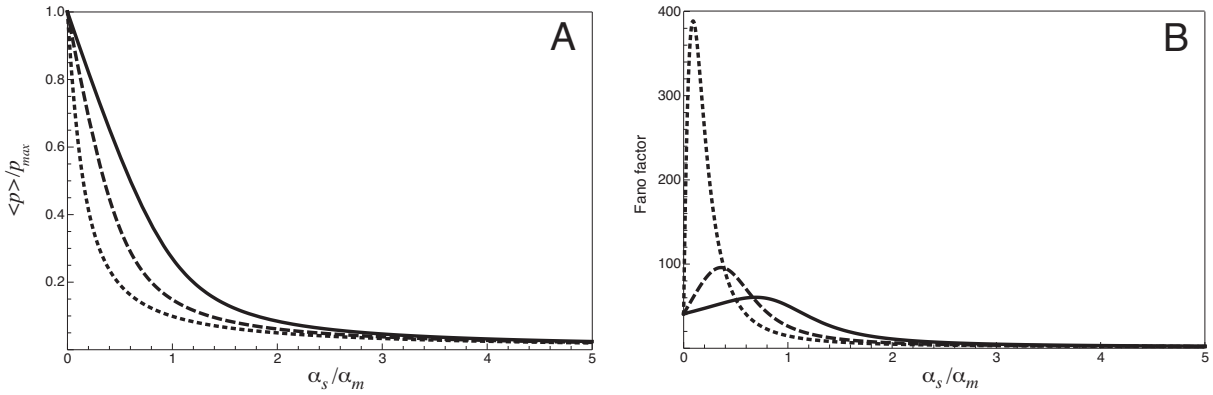


FIG. S5: Steady-state properties of the principal target proteins in absence of auxiliary targets when we consider a partial recycling of the srRNA. Mean protein level $\langle p\rangle/p_{max}$ (A) and Fano factor (B) as a function of the ratio $\alpha_s/\alpha_m$ for different values of the fraction $f$ of srRNA co-degraded with the principal target mRNA: $f = 1$ (full lines), 0.5 (dashed lines) and 0.1 (dotted lines). Fixed parameters as in Fig. S1.

given by

$$\frac{ds}{dt} = \alpha_s - \beta_s s - k_+ sm + k_- c_0 + (1-f)\beta_{c_0} c_0 + \xi_s + \xi_{k_+} + \xi_{k_-} + \xi'_{c_0}, \tag{B18}$$

$$\frac{dm}{dt} = \alpha_m - \beta_m m - k_+ sm + k_- c_0 + \xi_m + \xi_{k_+} + \xi_{k_-}, \tag{B19}$$

$$\frac{dc_0}{dt} = k_+ sm - k_- c_0 - \beta_{c_0} c_0 - \xi_{k_+} - \xi_{k_-} + \xi_{c_0}, \tag{B20}$$

$$\frac{dp}{dt} = \gamma m - \beta_p p + \xi_p, \tag{B21}$$

with $k_+$ the association rate between $s$ and $m$, $k_-$ the dissociation rate of $c_0$ and $\beta_{c_0} \gg k_-$ the active degradation rate of the complexes. The amplitude of the Langevin noise terms are: $N_{k_+} = k_+\langle s\rangle\langle m\rangle$, $N_{k_-} = k_-\langle c_0\rangle$, $N_{c_0} = \beta_{c_0}\langle c_0\rangle$ and $N'_{c_0} = \beta_{c_0}(1-f)\langle c_0\rangle$.

Substituting the steady-state mean value of $c_0$ ($\langle c_0\rangle = k_+\langle s\rangle\langle m\rangle/(k_- + \beta_{c_0})$) in Eq.B18 and B19 leads to the system

$$0 = \alpha_m - \beta_m\langle m\rangle - k\langle s\rangle\langle m\rangle \tag{B22}$$

$$0 = \alpha_s - \beta_s\langle s\rangle - kf\langle s\rangle\langle m\rangle \tag{B23}$$

with $k = k_+\beta_{c_0}/(k_- + \beta_{c_0})$. The mean gene expression of the principal targets is then given by

$$\langle p\rangle = \frac{1}{2\alpha_m}\left(\alpha_m - \alpha_s/f - \lambda' + \sqrt{[\alpha_m - \alpha_s/f - \lambda')^2 + 4\alpha_m\lambda'}\right) p_{max} \tag{B24}$$

with $\lambda' = \beta_s\beta_m/(fk)$. Thus, accounting for $f$ renormalizes the leakage rate $\lambda$ and the threshold position $\alpha_s/f$, but does not change the general shape of the linear-threshold response. Since a fraction of srRNA are recycled, for a fixed srRNA transcription rate, the regulation will be more efficient for smaller $f$ (Fig. S5A).

Fig. S5B shows a significant increase in the noise-to-signal ratio of the principal target proteins when the srRNA is highly recycled. Indeed, as the fluctuations of $s$ and $m$ are highly correlated in the ultra-sensitive cross-over regime [6, 21, 22], the intrinsic noise of the output proteins will suffer from the increase of the srRNA fluctuations due to the stochastic degradation of the complexes $c_0$.

### Appendix C: Steady-state properties with auxiliary targets

In this section, we discuss the impact of auxiliary target on steady-state properties of the principal targets.

### 1. Mean levels

Substituting the steady-state mean value of $c$ ($\langle c\rangle = k_a\langle s\rangle\langle n\rangle/(k_d+\beta_c)$) in Eq.A1 and A13, allows interpreting the auxiliary targets as stoichiometric weak targets of the srRNA with an effective interaction constant $k_{\text{eff}} = k_a p_d(\beta_c/k_d)/(1+\beta_c/k_d) \ll k$:

$$\frac{d\langle m\rangle}{dt} = 0 \;=\; \alpha_m - \beta_m\langle m\rangle - k\langle s\rangle\langle m\rangle \tag{C1}$$

$$\frac{d\langle s\rangle}{dt} = 0 \;=\; \alpha_s - \beta_s\langle s\rangle - k\langle s\rangle\langle m\rangle - k_{\text{eff}}\langle s\rangle\langle n\rangle \tag{C2}$$

$$\frac{d\langle n\rangle}{dt} = 0 \;=\; \alpha_n - \beta_n\langle n\rangle - \frac{k_{\text{eff}}}{p_d}\langle s\rangle\langle n\rangle \tag{C3}$$

The explicit solution of this system is quite cumbersome so we do not give its exact form here.

The level of auxiliary targets would start to play a significant role only when $k_{\text{eff}}\langle n\rangle \sim k\langle m\rangle$ [1], i.e when $\alpha_n \sim (k/k_{\text{eff}})\alpha_m \gg \alpha_m$. In this situation, the auxiliary targets modify the steady-state level of the srRNA and then indirectly the one of the principal target. This could help to finely tune the position of the transition between repressed and unrepressed regime (Fig.2A of the main text) but this effect does not change the regulatory logic of the post-transcriptional regulation.

In the following we focus on the regime where the auxiliary targets have a negligible effect on the steady-state mean levels of the free srRNAs and of the principal targets.

### 2. Fluctuations

To appreciate the effect of auxiliary targets on the fluctuations of principal targets, we first simplify the model by assuming that auxiliary targets have no effect on the mean steady-state level of principal targets ($\beta_c/k_d \to 0$). Effects of a finite $\beta_c$ on the fluctuations are briefly discussed in the end of Sec.C 3. Results are obtained, as previously, within the linear noise approximation.

Applying the Fourier transform method to $n$ and $c$ (Eqs. A13 and A14), we find expressions for $\delta\tilde{n}$ and $\delta\tilde{c}$ as a function of $\delta\tilde{s}$. Substituting these expressions in the linearized Fourier equation for $s$ gives

$$\delta\tilde{s} = \frac{-k\langle s\rangle\delta\tilde{m} + \xi_s + \xi_k + \imath\omega\frac{(\imath\omega+\beta_n)}{E}(\xi_a+\xi_d) - \imath\omega\frac{k_a\langle s\rangle}{E}\xi_n}{\beta_s + \imath\omega(k_a\langle n\rangle)\frac{(\imath\omega+\beta_n)}{E} + k\langle m\rangle}, \tag{C4}$$

with $E = (\imath\omega+k_d)(\imath\omega+\beta_n) + \imath\omega k_a\langle s\rangle$.

For high numbers of auxiliary targets ($\langle n\rangle/K_d \gg 1$), Eq.C4 leads to

$$\langle|\delta\tilde{s}|^2\rangle \approx \langle s\rangle\frac{\Omega}{D\ell}. \tag{C5}$$

The fluctuations due to the interaction with the principal targets ($-k\langle s\rangle\delta\tilde{m}$ and $\xi_k$) as well as those due to the srRNA production (including transcriptional burstiness) and degradation ($\xi_s$) have been absorbed by the large pool of complexed srRNAs, leaving only the contribution due to diffusion noise. Since fluctuations of $s$ propagate in those of $m$ and $p$, the Fano factor is given by

$$\nu = 1 + b\left[\frac{1+(k^2\langle m\rangle\langle s\rangle/\alpha_m)(2\langle m\rangle+\langle s\rangle)(\Omega/2D\ell)}{1+k\langle s\rangle/\beta_m}\right]. \tag{C6}$$

For high diffusion constant, this expression reduces to $\nu = 1+b^*$. Note that unlike the case with no auxiliary target, where this expression was only valid in the repressed regime (see Eq.B16), here the reduction of fluctuations holds for any level of the srRNA.

For an arbitrary number of auxiliary targets, no simple expression can be found for $\nu$. Figures 2 B,C of the main text show numerical results of the Fano factor for different values of the parameters.

It should be noted that the relevant parameter here is not $\langle n\rangle$ but $\langle n\rangle/K_d$, since the efficacy of the fluctuation absorption depends on the size of the complexed pool ($\langle c\rangle = (\langle n\rangle/K_d)\langle s\rangle$). Changing $\alpha_n$, $\beta_n$, $k_a$ and $k_d$ while keeping $\langle n\rangle/K_d$ constant does not impact significantly on the behavior of the process.

As before, Fig. S3B shows the remarkable ability of the LNA to describe the general behavior of post-transcriptional regulation in presence of auxiliary targets.

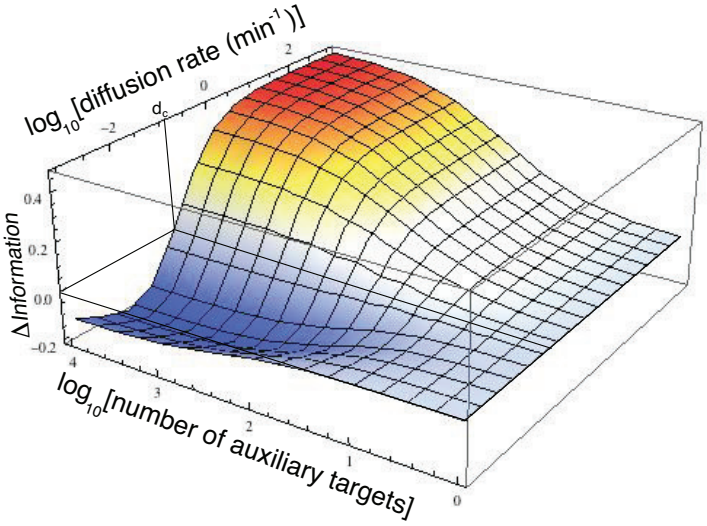


FIG. S6: Change in the information capacity due to the presence of auxiliary targets, for different values of the diffusion rate $d = D\ell/\Omega$. Same parameters as in Fig. S2

### 3. Information capacity

In the last section we saw that interactions with auxiliary targets reduce or increase the noise-to-signal ratio, depending on the importance of diffusion noise in the system. Next we aimed to quantify the impact of these results on the function of the srRNA regulatory pathway. Motivated by its recent successful applications to gene regulation [25–28], we decide to focus on the capacity of this pathway to convey information.

In information theory, transfer of information between an input $X$ and an output $Y$ via a given channel is well-characterized by the concept of mutual information [29]:

$$I(X;Y) = \int dX \int dY\, P(X,Y) \log_2 \left[ \frac{P(X,Y)}{P(X)P(Y)} \right], \tag{C7}$$

where $P(X,Y)$ is the joint probability distribution function of $X$ and $Y$, $P(X)$ and $P(Y)$ are the marginal probability distribution functions. Intuitively, the mutual information represents the number of different output levels achievable by varying the input, and depends on the intrinsic noise properties of the channel. The maximal mutual information with respect to the distribution of inputs is called the information capacity of the channel.

Since biological circuits could be seen as information channel between environmental or internal signals and internal responses, information theory concepts have been recently applied to genetic networks. It can be shown [25, 26] that the information capacity of such circuit could be approximated, in the low-noise limit, by

$$I_{\max} = \log_2 \left( \frac{1}{\sqrt{2\pi e}} \int dX \left| \frac{d\langle Y \rangle(X)}{dX} \right| \frac{1}{\sigma_Y(X)} \right), \tag{C8}$$

with $\sigma_Y^2$ the variance of the output for a given input level. The information capacity therefore depends directly on the variation in the mean output level in response to a change in the input level and on the intrinsic noise properties of the channel (via $\sigma_Y$). For example, a system with a flat or a very noisy response cannot carry information, and would have a low information capacity.

#### a. *Effect of auxiliary targets*

We use Eq.C8 to estimate the global effect of auxiliary targets and diffusion on the information capacity of the srRNA post-transcriptional regulation. We define the input as the transcription rate $\alpha_s$ of the srRNA and the output as the protein level $p$. Fig. S6 shows the effect of auxiliary targets on the information capacity of the srRNA regulation. For slow transport, diffusion noise dominates and the information capacity is reduced by an increase of the number of targets. In contrast, for fast transport, the pool of complexed srRNA allows an efficient absorption of the srRNA

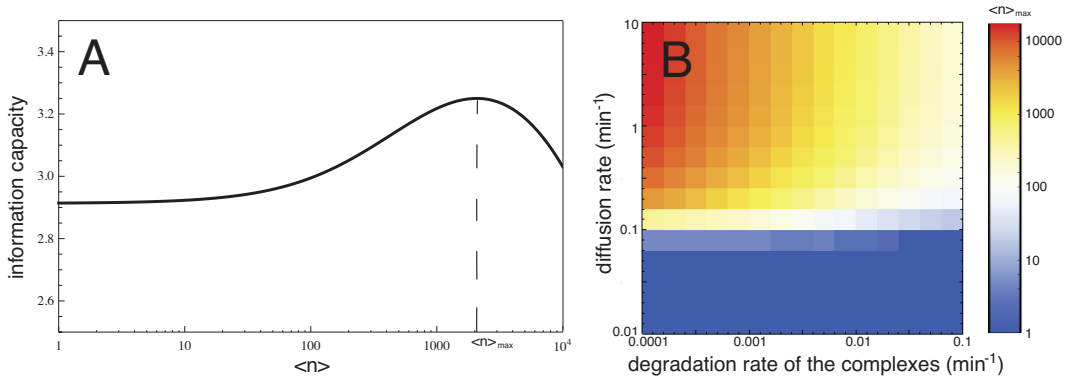


FIG. S7: Limitation of information gain due to the degradation of the complex when $d > d_c$. (A) Information capacity as a function of the number of auxiliary targets ($d \to \infty$, $\beta_c = 1/200$). (B) Number of auxiliary targets optimizing the information capacity as a function of the diffusion rate $d$ and of the degradation rate $\beta_c$ of the complexes. Same fixed parameters as in Fig. S2.

fluctuations in the crossover region, and promotes a good information transfer. More precisely, there exists a value for the diffusion parameter $d \equiv D\ell/\Omega$ such that, for $d > d_c$, adding auxiliary targets in the system decreases globally the intrinsic noise of the output protein and improve the information capacity of the post-transcriptional regulation; for $d < d_c$, auxiliary targets increase the output noise and the information transmission is less efficient.

The value of $d_c$ depends on the different parameters of the system in a non trivial way, as shown in Fig. S2. As expected the value of the production rate of the principal targets does not influence the position of the transition (Fig. S2 C), since $\alpha_m$ mainly defined the position of the different regulation regimes but not the general behavior of the process. More surprisingly, $d_c$ does not depend significantly on the microscopic reaction rate $k^0$ (Fig. S2 D).

The main contribution comes from the srRNA and mRNA turnover rates (Fig. S2 A,B). Since $\beta_m$ controls the strength of the diffusion noise of the srRNA-mRNA interaction (see Eq.B17), high mRNA degradation rate will have an impact on $d_c$. Regarding $\beta_s$ we note that at the transition the fluctuations of the srRNA with (see Eq.C5) or without ($\langle|\delta\tilde{s}|^2\rangle \sim \langle s\rangle/\beta_s$) auxiliary targets have the same amplitude. This implies that $\beta_s \sim d$. Therefore, increasing $\beta_s$ reduces the influence of burstiness absorption, and diffusion noise starts to dominate at higher values of the diffusion constant.

When the srRNA transcription is highly bursty, one gain in information capacity even at slow diffusion (Fig. S2 E). This is due to buffering of transcriptional noise, which is higher for a bursty promoter, by the auxiliary targets. Diffusion noise, however, does not depend on the nature of the transcription process. Thus, for bursty promoters the advantage of auxiliary targets surpasses the disadvantage dues to diffusion noise even at slow diffusion.

### *b. Effect of the degradation of the complex*

The previous part suggests that if $d > d_c$, the more auxiliary targets the better. However, as explained in Sec.C 1, at high number of auxiliary targets, the level of the free srRNAs and therefore that of the principal targets become influenced by the presence of the auxiliary targets due to the (slow but finite) degradation of the complexes. If we set $\beta_c$ to a non-zero value, in addition to affect the fluctuations ($\sim \sigma_Y$) of principal targets, the number of auxiliary targets will also influence the sensitivity of the regulatory logic of the principal targets ($\sim d\langle Y\rangle/dX$). Therefore, from Eq.C8 we expect a change in the behavior of the information capacity as a function of $n$. While the boundary between slow and fast transport mode does not significantly depend on the degradation rate of the complex (Fig. S7B), information capacity in the fast diffusion regime exhibits a maximum at a finite number of auxiliary targets (Fig. S7A). This then defines an upper limit for the number of auxiliary targets that improves the information transfer. Auxiliary targets act also as kinetic traps for the srRNAs and slow-down the regulation process, as discussed below, imposing a stronger bound on the number of auxiliary targets.

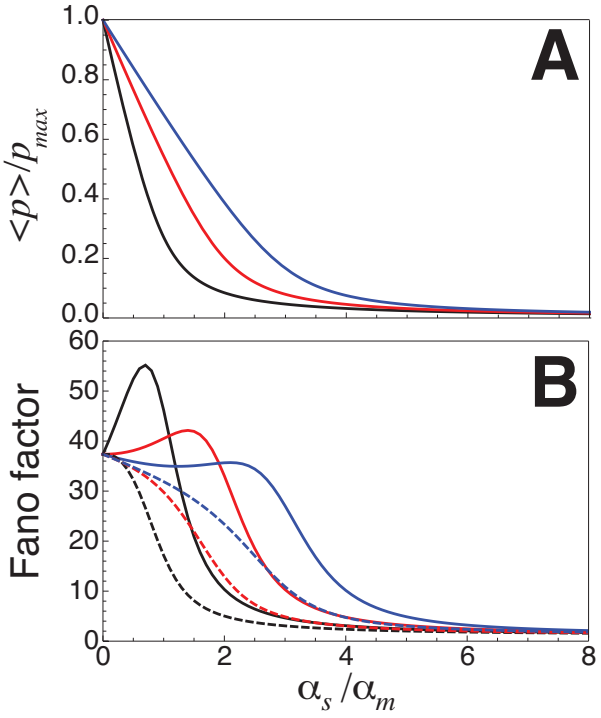


FIG. S8: Impact of strong auxiliary targets on the steady-state mean (A) and Fano factor (B) of the principal targets for $\alpha_a/\alpha_m = 0$ (black), 1 (red) and 2 (blue), in absence (full lines) or in presence (dashed lines) of weak auxiliary targets. Fixed parameters as in Fig. S1

### c. *Effect of recycling the srRNA*

We saw in section B 3 that the partial recycling of the srRNA during the degradation of the complex srRNA-principal mRNA increased the intrinsic fluctuations of the principal targets. Therefore, as in the situation of a bursty srRNA transcription, one gain in information capacity even at slow diffusion (Fig. S2 F). Indeed, auxiliary targets buffer the intrinsic noise of the free srRNAs which is more important at low $f$, and diffusion noise does not impact the degradation of the complex $c_0$. Thus, the advantage of auxiliary targets surpasses the disadvantage due to diffusion noise even at slow diffusion.

## 4. Effect of strong auxiliary targets

In our work, we have identified the principal targets with the few strongly affected targets. However, some of these targets may not be phenotypically relevant and may be defined as "strong auxiliary" targets [30]. In this section, we briefly discuss the effect of such targets on the steady-state properties of the principal targets by augmenting our set of Langevin equations by

$$\frac{dm_a}{dt} = \alpha_a - \beta_m m_a - ks\, m_a + \xi_a + \xi_{ka} \tag{C9}$$

with $m_a$ the number of strong auxiliary mRNAs.

Fig. S8A shows that strong auxiliary targets have a significant impact on the regulatory logic of principal targets, shifting the threshold position ($\alpha_s \sim \alpha_m + \alpha_a$) to higher values. They play a role a sponge by sequestering the srRNA molecules away from the principal targets and therefore delaying the entry in the silenced regime.

However, Fig. S8B illustrates that the buffer effect played by weak auxiliary targets is not perturbed by the presence of strong auxiliary targets.

## Appendix D: Kinetic properties

In this section, we describe the numerical method used to compute the first passage time (FPT) statistics. We also present results on FPT if we account for diffusion noise.

### 1. Method

We use the Gillespie algorithm [23] to sample exact stochastic trajectories of the process where, for simplicity, we neglect fluctuations in the total number of auxiliary targets $n_{\rm tot}$. Each simulation starts with a configuration sampled from the steady state distribution of principal targets (Poissonian distribution with mean $\alpha_m/\beta_m$). At $t = 0$ the transcription of srRNA is switched on, and the kinetic response is assessed by measuring the statistics of the first passage time when the number of principal targets reaches zero.

### 2. Effect of diffusion

To estimate the effect of diffusion on the first-passage time distribution, we use the linear-noise approximation (see Sec.B 2 a). In the LNA, fluctuations around the mean are assumed to be small and normally distributed [9]. The total probability $P(m, s, c; t)$ to observe the microstate $(m, s, c)$ at time $t$ is then given by a multivariate normal distribution

$$P(m, s, c; t) = \frac{1}{(2\pi)^{3/2}|det[C(t)]|^{1/2}} \exp[-X(t)^\dagger C^{-1}(t)X(t)/2], \tag{D1}$$

with the vector $X = (m - \langle m\rangle(t); s - \langle s\rangle(t); c - \langle c\rangle(t))$. The evolution of the covariance matrix $C(t)$ follows Eq.B11. Denoting $S_{m_0}(t) = \int_{m_0}^{\infty} dm \int dsdc\, P(m, s, c; t)$ the probability for $m$ to be larger than $m_0$ at time $t$, the first-passage time probability $h_{m_0}(t)$ at $m_0$ is given by

$$h_{m_0}(t) = \frac{-\frac{d}{dt}\left[S_{m_0}(t)\right]}{S_{m_0}(0) - S_{m_0}(\infty)}. \tag{D2}$$

Fig. S3C shows the very good agreement between results from the LNA and those from the Gillespie algorithm for the time evolution of the mean and the variance of $m$. However, the distribution of the FPT to reach $m_0 = 0$ predicted by the LNA has a long tail which dramatically increases (by almost 8 times) the predicted variance for the FPT (see Fig. S3D). This underlines the limits of the LNA to describe the exact probability distribution functions in systems with small number of particles.

In order to study the effect of diffusion on the FPT distribution, we place ourselves in a regime where the LNA should well characterize also the first-passage time. We choose higher production rates for $m$ and $s$ ($\alpha_m = 5$ min$^{-1}$, $\langle m\rangle(0) = 50$ and $\alpha_s = 50$ min$^{-1}$) and we study the first-passage time to reach $m_0 = \langle m\rangle(0)/2 = 25$. The inset in Fig. S3D confirms the success of the LNA in this regime.

Fig. S9A and B show the mean and variance of the FPT as a function of the diffusion rate and of the number of auxiliary targets. Low diffusion rates exhibit higher mean and variance. Even for a small number of auxiliary targets where the mean response of the srRNA-repression outperforms the one of the TF-like repression, the uncertainty of the response in the slow transport mode could be very large.

The entire probability distribution function for the FPT as a function of the diffusion rate is shown in Fig. S9C, D and E. For fast diffusion, as expected, the distributions are well peaked around a mean value, which increases with the number of auxiliary targets. When the diffusion is slow, however, all interactions become diffusion limited, and diffusion dominates the noise. In this limit the distribution is peaked at short first-passage times, due to possible avoidance of the auxiliary targets, but exhibits a long tail, due to possible long searches for the principal targets.

## Appendix E: Conservation of microRNA targets

In this section we briefly describe the methods used to analyze the evolutionary data on microRNA targets.

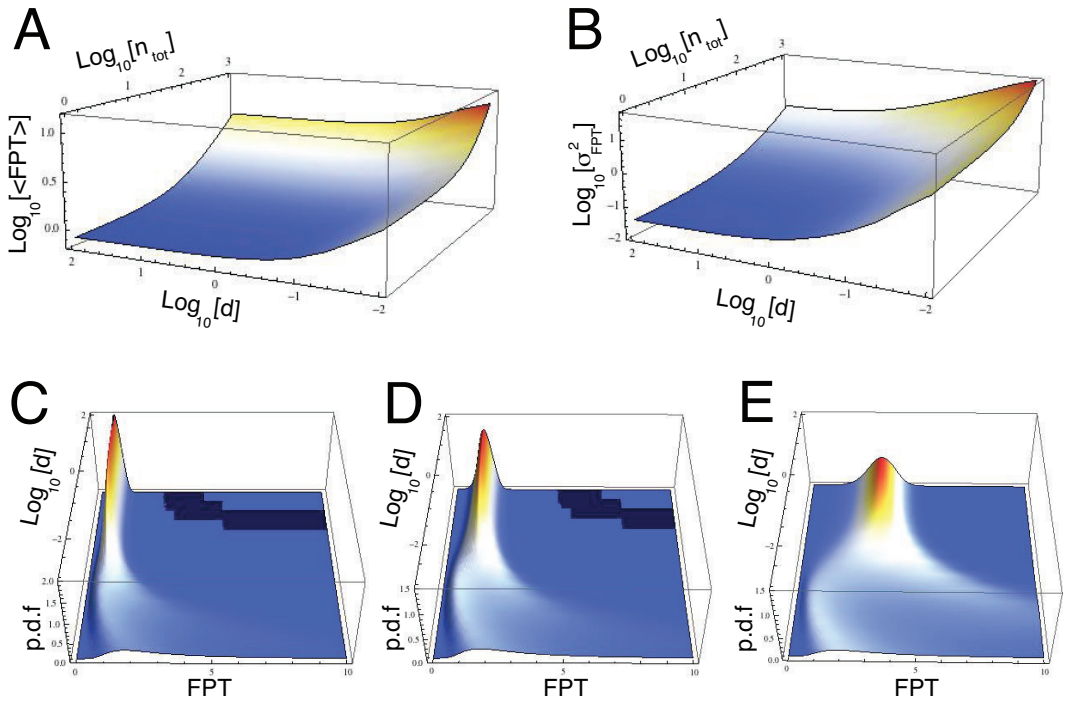


FIG. S9: Effect of diffusion on the kinetic response of srRNA regulation. Mean (A) and variance (B) of the first-passage time (FPT) as a function of the diffusion rate $d = D\ell/\Omega$ and of the number of auxiliary targets $n_{\rm tot}$. And probability distribution function (p.d.f) of the FPT as a function of the diffusion rate for $n_{\rm tot} = 0$ (C), 100 (D) and 500 (E). Results were obtained using the linear-noise approximation. Same fixed parameters as in Fig. S3.

### 1. Data set

We study the conservation of microRNA targets on a set of 87 microRNA families conserved among vertebrates (Dataset S1). The dataset, including sequences of seed regions and mature species for each microRNA in each of the 12 studied vertebrate genomes, was downloaded from the TargetScan web site (www.targetscan.org). The list of aligned 3'UTRs (corresponding to 30,887 genes) needed to search for target sites was downloaded from the same website.

As a control, we performed parallel analysis on a set of 1,000 "mock" microRNAs (Dataset S2). The mature sequences of the mock microRNAs were constructed by randomly picking one of the 87 natural mature sequences, and replacing the seed regions by randomly generated sequence having the same dinucleotide composition as the seed regions of the 87 natural microRNAs (Fig. S10).

### 2. Analysis

#### *a. Defining target sites and conservation score*

We used the TargetScan algorithm (implemented as perl script, available for download from the TargetScan website) to obtain the list of putative binding sites for each microRNA (real or mock) in the corresponding genome. The list of gene targets of a particular microRNA is defined as the list of all genes that have at least one putative binding sites of that microRNA in their 3'UTR. Fig. S11 shows that for all species the distributions of target numbers is similar for real and random seeds.

To investigate the conservation of the number of targets across species, we normalize the predicted number of targets $N_{i,s}$ per microRNA $i$ in each species $s$ by the total number of genes per species $N_{tot,s}$ in the alignment. This allows to correct for the loss of gene homologs as the evolutionary distance with human increases. The relative fluctuation of the number of targets for the microRNA $i$ across species is then defined as the ratio between the standard deviation and the mean of the ensemble of values for $N_{i,s}/N_{tot,s}$ ($s$=human, chimpanzee,..., frog).

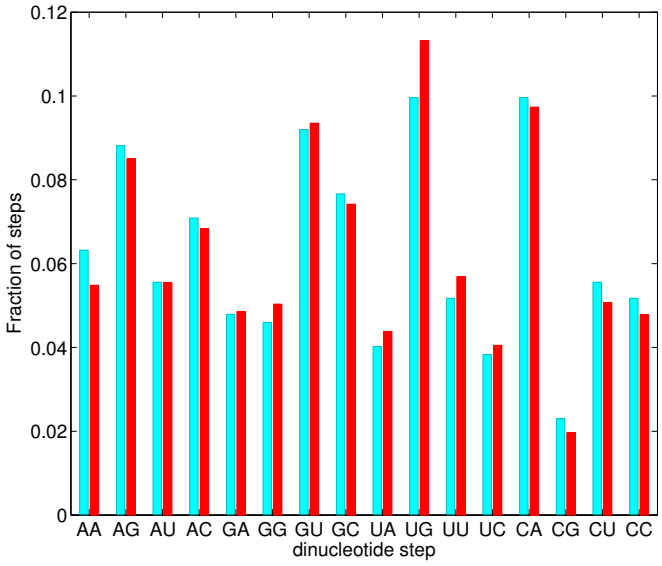


FIG. S10: Dinucleotide composition of the seed regions of the 87 natural microRNAs (blue bars) and of the 1,000 fake microRNAs (red bars).

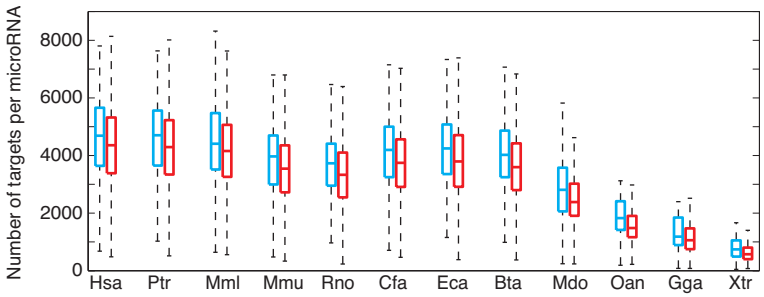


FIG. S11: Boxplots of the number of targets per microRNA in human (Hsa), chimpanzee (Ptr), rhesus (Mml), mouse (Mmu), rat (Rno), dog (Cfa), horse (Eca), cow (Bta), opossum (Mdo), platypus (Oan), chicken (Gga) and frog (Xtr), for natural (blue) and fake (red) microRNAs.

Taking the list of human targets as reference, we represent the predictions of Targetscan by a binary array $x^t_{i,s}$, where $x^t_{i,s} = 1$ if gene $t$ is a target of microRNA $i$ in human and in species $s$, and 0 otherwise. The observed frequency $f^t_i$ of $t$ for microRNA $i$ is then defined as the mean value of $x^t_{i,s}$ across the species

$$f^t_i = \frac{1}{11} \sum_{s \neq \text{human}} x^t_{i,s}. \tag{E1}$$

We exclude human from the sum since $x^t_{i,s}$ is always equal to 1 in human by definition. To estimate the conservation of a human target in vertebrates, we define a conservation score $C^t_i$ as the ratio between $f^t_i$ and the background frequency $f^t_0$ ($C^t_i = f^t_i / f^t_0$) where $f^t_0 = (1/11) \sum_{s \neq \text{human}} \delta_{t,s}$ with $\delta_{t,s} = 1$ if gene $t$ is present in species $s$, 0 otherwise. $f^t_0$ represents an upper bound for $f^t_i$. For example, $C^t_i = 1$ means that gene $t$ is a target of microRNA $i$ in every species where $t$ is present. This target-dependent normalization of $f^t_i$ permits unbiased comparisons between all the genes even if some are not present in every species.

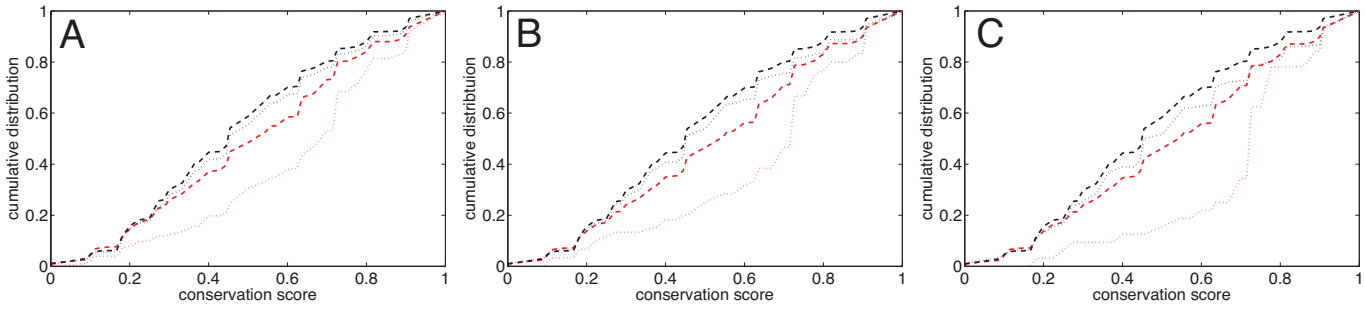


FIG. S12: Same as in Fig. 6B of the main text but for different definitions of the strong and weak ensembles. The limit (in $\log_2$ of the fold-change) is fixed to $-0.4$ (A), $-0.8$ (B) or -1 (C).

### *b. Conservation of weak and strong targets*

To investigate the conservation of principal and auxiliary targets, we use published experimental data that measured global proteome response to transfection of a microRNA (miR-1, miR-124 and miR-181) in (human) HeLa cells [31]. For each transfected microRNA, we extract from the experimental dataset the protein level change of each of its target genes (as defined above), if it had been measured. Dataset S3 contains the list of these genes for miR-1 (382 genes), miR-124 (249 genes) and miR-181 (345 genes), as well as the corresponding fold-change in protein level (in $\log_2$ unit).

The distribution of fold-repression does not offer a natural separation between principal and auxiliary targets in HeLa cells. We therefore split the targets based on their fold-change into an subset of "strong targets", representing targets with a fold-repression below a given arbitrary limit ($\log_2$ of the fold-change $\leq -0.6$) and the complementary subset of "weak targets". We choose this arbitrary limit in order to have enough statistics for the strong target ensemble. We verified that our conclusions do not depend on the choice of this limit (see Fig. S12).

For each gene $t$ of a given subset (weak or strong), we estimate its conservation scores relatively to the transfected natural microRNAs, or to the random microRNAs (($\{C_i^t\}$ for $i \in$ {miR-1, miR-124, miR-181} or $i \in$ {random seeds}). Comparisons between the corresponding distributions of conservation scores allows to check the specificity of conservation properties of weak and strong targets of natural microRNAs.

## Appendix F: Parameters used in the main text

Typical values for parameters are only known for bacterial srRNA pathways [1, 4]. Therefore, we choose to use these ranges of values to plot our figures. However, Fig. S2 shows that the effects described in the paper are robust over a wide range of parameters values which likely also includes the eukaryotic pathways.

### 1. Figure 2 A

Fixed parameters are (in min-1) $\alpha_m = 1$, $\beta_m = \beta_s = 0.1$, $\gamma = 4$, $\beta_p = 1/200$, $k = 0.1$, $k_a = k$, $k_d = 1$, $\beta_n = 0.1$, $\beta_c = 1/200$, $p_d = 1/20$.

### 2. Figures 2 B,C and 3

Fixed parameters are (in min-1) $\alpha_m = 1$, $\beta_m = \beta_s = 0.1$, $\gamma = 4$, $\beta_p = 1/200$, $\beta_n = 0.1$, $\beta_c = 0$, $k^0 = 0.1$, $k_a^0 = 0.1$, $k_d^0 = 1$, $d = \infty$ ( A) or 0.05 (B).

### 3. Figures 4 and 5

Fixed parameters are (in min-1) $\alpha_m = 1$, $\alpha_s = 10$, $\beta_m = \beta_s = 0.1$, $k = k_a = 0.1$, $k_d = 1$.

---


[1] Levine, E., Zhang, Z., Kuhlman, T., and Hwa, T. Quantitative characteristics of gene regulation by small rna. *PLoS Biol* **5**(9), e229, Sep (2007).

[2] Mitarai, N., Andersson, A. M. C., Krishna, S., Semsey, S., and Sneppen, K. Efficient degradation and expression prioritization with small rnas. *Phys Biol* **4**(3), 164–171, Sep (2007).

[3] Mitarai, N., Benjamin, J.-A. M., Krishna, S., Semsey, S., Csiszovszki, Z., Massé, E., and Sneppen, K. Dynamic features of gene expression control by small regulatory rnas. *Proc Natl Acad Sci U S A* **106**(26), 10655–10659, Jun (2009).

[4] Shimoni, Y., Friedlander, G., Hetzroni, G., Niv, G., Altuvia, S., Biham, O., and Margalit, H. Regulation of gene expression by small non-coding rnas: a quantitative view. *Mol Syst Biol* **3**, 138 (2007).

[5] Jost, D., Nowojewski, A., and Levine, E. Small rna biology is systems biology. *BMB Rep* **44**(1), 11–21, Jan (2011).

[6] Mehta, P., Goyal, S., and Wingreen, N. S. A quantitative comparison of srna-based and protein-based gene regulation. *Mol Syst Biol* **4**, 221 (2008).

[7] Gottesman, S. Micros for microbes: non-coding regulatory rnas in bacteria. *Trends Genet* **21**(7), 399–404, Jul (2005).

[8] Ghildiyal, M. and Zamore, P. D. Small silencing rnas: an expanding universe. *Nat Rev Genet* **10**(2), 94–108, Feb (2009).

[9] van Kampen, N. *Stochastic Processes in Physics and Chemistry*. North-Holland, Amsterdam, (2001).

[10] Chubb, J. R., Trcek, T., Shenoy, S. M., and Singer, R. H. Transcriptional pulsing of a developmental gene. *Curr Biol* **16**(10), 1018–1025, May (2006).

[11] So, L.-H., Ghosh, A., Zong, C., Sepúlveda, L. A., Segev, R., and Golding, I. General properties of transcriptional time series in escherichia coli. *Nat Genet* **43**(6), 554–560, Jun (2011).

[12] Golding, I., Paulsson, J., Zawilski, S. M., and Cox, E. C. Real-time kinetics of gene activity in individual bacteria. *Cell* **123**(6), 1025–1036, Dec (2005).

[13] Paré, A., Lemons, D., Kosman, D., Beaver, W., Freund, Y., and McGinnis, W. Visualization of individual scr mrnas during drosophila embryogenesis yields evidence for transcriptional bursting. *Curr Biol* **19**(23), 2037–2042, Dec (2009).

[14] Bialek, W. and Setayeshgar, S. Physical limits to biochemical signaling. *Proc Natl Acad Sci U S A* **102**(29), 10040–10045, Jul (2005).

[15] Berg, O. G. On diffusion-controlled dissociation. *Chemical Physics* **31**(1), 47 – 57 (1978).

[16] Berg, H. C. and Purcell, E. M. Physics of chemoreception. *Biophys J* **20**(2), 193–219, Nov (1977).

[17] Tkacik, G. and Bialek, W. Diffusion, dimensionality, and noise in transcriptional regulation. *Phys Rev E Stat Nonlin Soft Matter Phys* **79**(5 Pt 1), 051901, May (2009).

[18] Thattai, M. and van Oudenaarden, A. Intrinsic noise in gene regulatory networks. *Proc Natl Acad Sci U S A* **98**(15), 8614–8619, Jul (2001).

[19] Elowitz, M. B., Levine, A. J., Siggia, E. D., and Swain, P. S. Stochastic gene expression in a single cell. *Science* **297**(5584), 1183–1186, Aug (2002).

[20] Paulsson, J. Summing up the noise in gene networks. *Nature* **427**(6973), 415–418, Jan (2004).

[21] Elf, J., Paulsson, J., Berg, O. G., and Ehrenberg, M. Near-critical phenomena in intracellular metabolite pools. *Biophys J* **84**(1), 154–170, Jan (2003).

[22] Levine, E., Huang, M., Huang, Y., Kuhlman, T., Zhang, Z., and Hwa, T. On noise and silence in gene regulation by small rna. (2008).

[23] Gillespie, D. Exact stochastic simulation of coupled chemical reactions. *J Phys Chem* **81**, 2340–2361 (1977).

[24] Hao, Y., Xu, L., and Shi, H. Theoretical analysis of catalytic-srna-mediated gene silencing. *J. Mol. Biol.* **406**, 195–204 (2011).

[25] Tkacik, G., Callan, C. G., and Bialek, W. Information flow and optimization in transcriptional regulation. *Proc Natl Acad Sci U S A* **105**(34), 12265–12270, Aug (2008).

[26] Tkacik, G., Walczak, A. M., and Bialek, W. Optimizing information flow in small genetic networks. *Phys Rev E Stat Nonlin Soft Matter Phys* **80**(3 Pt 1), 031920, Sep (2009).

[27] Walczak, A. M., Tkacik, G., and Bialek, W. Optimizing information flow in small genetic networks. ii. feed-forward interactions. *Phys Rev E Stat Nonlin Soft Matter Phys* **81**(4 Pt 1), 041905, Apr (2010).

[28] Mugler, A., Grinshpun, B., Franks, R., and Wiggins, C. H. Statistical method for revealing form-function relations in biological networks. *Proc Natl Acad Sci U S A* **108**(2), 446–451, Jan (2011).

[29] Cover, T. and Thomas, J. *Elements of Information Theory*. John Wiley and Sons, (1991).

[30] Flynt, A. S. and Lai, E. C. Biological principles of microrna-mediated regulation: shared themes amid diversity. *Nat Rev Genet* **9**(11), 831–842, Nov (2008).

[31] Baek, D., Villén, J., Shin, C., Camargo, F. D., Gygi, S. P., and Bartel, D. P. The impact of microrna on protein output. *Nature* **455**(7209), 64–71, Sep (2008).